Convection forced by a descending dry layer and low-level moist convergence

By ANDREW RUSSELL[1][⋆], GERAINT VAUGHAN[1], EMILY G. NORTON[1], HUGO M. A. RICKETTS[1], CYRIL J. MORCRETTE[2], TIM J. HEWISON[2], KEITH. A. BROWNING[3] and ALAN M. BLYTH[3]

[1]*Centre for Atmospheric Science, University of Manchester, UK;* [2]*Met Office, Exeter, UK;*[3]*School of Earth and Environment, University of Leeds, UK*

ABSTRACT

A narrow line of convective showers were observed over southern England on 18 July 2005 during the Convective Storm Initiation Project. The showers formed behind a cold front (CF), beneath two apparently descending dry layers (i.e. sloping so that they descended relative to the instruments observing them). The lowermost dry layer was associated with a tropopause fold from a depression, which formed 2 days earlier from a breaking Rossby wave, located north-west of the UK. The uppermost dry layer had fragmented from the original streamer due to rotation around the depression. (This rotation was also responsible for the observations of apparent descent — ascent would otherwise be seen behind a CF.) The lowermost dry layer descended over the UK and overran higher θ_w air beneath it, resulting in potential instability. Combined with a surface convergence line (which triggered the convection but had less impact on the convective available potential energy than the potential instability), convection was forced up to 5.5 km where the uppermost dry layer capped it. The period when convection was possible was very short, thus explaining the narrowness of the shower band. CSIP observations and model data are presented to illustrate the unique processes in this case.

1 Introduction

1.1 Convective storms in the UK and CSIP

Convective storms are difficult to predict and can have severe impacts. For example, the storm that caused the Boscastle flood, which occurred in the UK during the summer of 2004, developed quickly and caused great damage and disruption (Golding et al., 2005). The mechanisms that force the development of such storms are well understood at the conceptual level (Bennett et al., 2006). However, in practice, the observational network is not dense enough to study the development of convection in detail or to make use of this understanding and improve numerical model prediction (NWP) using increasing model resolution. (This latter point is less relevant for mesoscale processes that often develop within the domain of the highest resolution models, such as surface convergence lines (e.g. Morcrette et al., 2007), than for synoptic features that move into mesoscale domains and this will be important in determining the focus of this paper.)

In response to the need to improve the representation of these storms in numerical models, a greater understanding of the exact conditions leading to their initiation is required. This knowledge can be acquired by the execution of dedi-

cated field campaigns to observe these storms as they form. This paper focuses on data collected from one case during such a campaign: the Convective Storm Initiation Project (CSIP). The overall project is summarised by Browning et al. (2007) and, to date, detailed analysis from CSIP has shed light on the following subjects: secondary initiation of convection forced by gravity waves (Morcrette et al., 2006; Marsham and Parker, 2006); the varying ability of the UK Met Office Unified Model (UM; Cullen, 1993) in predicting the development of convective storms over the UK in different cases (Clark and Lean, 2006); the initiation of an isolated storm forced by a topographically induced convergence line and an upper-level potential vorticity (PV) anomaly (Morcrette et al., 2007); the role of cirrus shading in convective storm initiation (Marsham et al., 2007a) and in boundary layer development (Marsham et al., 2007b); and how the origin of an atmospheric lid was related to a breaking Rossby wave over the Atlantic via the physical descent of upper-level air down the resultant tropopause fold (Russell et al., 2008). In this paper, we will describe a case where an apparently descending double layer of stratospheric/upper-tropospheric air developed from a large upper-level PV anomaly and show how it contributed to the initiation of convection over the UK. Whilst neither of these layers can strictly be called "tropopause folds" as there is no evidence of the dynamical tropopause (i.e. the 2 PVU contour) folding back on itself, they are very similar in structure and identical in origin to such folds.

⋆ Corresponding author.
e-mail: andrew.russell-2@manchester.ac.uk

It is important to understand this particular case as the UK Met Office UM simulations of it failed to represent much of the detail of the convective showers. This point is discussed further in Section 7 of the paper but in the preceding sections we will show how the PV structure influencing the convection in this case was particularly complex. As a result, the model struggled to represent the more subtle aspects of this case, especially as the main PV features developed outside the model's mesoscale domain. This is a crucial point with the goal of improving precipitation forecasts in mind. It should be noted at this point that the convection in this case was triggered by a surface convergence line but, as these features are very well understood in the literature (Bennett et al., 2006; Morcrette et al., 2007, and references therein) and are usually well modelled, including this case, we will examine the upper-level features in much greater detail in this paper.

1.2   Upper-level forcing of convection

Hoskins et al. (1985) reviewed the mechanisms by which upper-level PV anomalies can reduce the convective stability of the troposphere. Usually, of greatest relevance is how the upward (downward) curvature of isentropes in the troposphere (stratosphere) associated with a moving PV anomaly is associated with tropospheric ascent ahead of, and descent of air behind, the depressed tropopause. It is this vertical displacement of the isentropic surfaces that causes the reduction in static stability beneath the PV anomaly and, under certain conditions, can induce convection (e.g. Griffiths et al., 2000; Morcrette et al., 2007).

Convection can also become more likely when upper-level air descends into the troposphere: when low wet-bulb potential temperature (θ_w) air from upper-levels overruns higher θ_w air nearer the surface, potential, or convective, instability is created. Potential instability is important because an unsaturated atmospheric column with θ_w decreasing with height will become unstable if it is lifted to saturation. For example, Browning and Roberts (1994; 1995) presented a case where an upper-level cold front (UCF) of low θ_w ran ahead of the higher θ_w air in advance of the surface cold front (SCF) — the region in between the two features was characterised by potential instability and convective storms were observed in that region. In such cases, the UCF often originates in the region behind the SCF where upper-level (usually dry) air is drawn in from the tropopause depression associated with the low driving the SCF. This flow of dry air is known as the "dry intrusion" (Browning, 1997) and it forms by the flow of upper-level (stratospheric or upper-tropospheric) air down the disturbed isentropic surfaces of the tropopause fold associated with the PV anomaly (Danielsen, 1964; 1968). As a further example of how such features influence convection, Vaughan et al. (1994) have presented a case where the flow of air from a tropopause depression started over the UK and extended into a cut-off low (COL) over Spain. In that case, satellite images showed arcs of convection to the west of Morocco, which was at the leading edge of the descending and anticylonically-curving flow initiated from the tropopause depression. Elsewhere in that case, deep convection was observed in the eastern sector of the COL (over eastern Spain) highlighting the impact of such descending upper-level features on the wider region around the tropopause depression. The investigation in the present paper is particularly interesting as there are no obvious examples of the role of multiple/concurrent stratospherically derived dry layers in cases of the initiation of convection in the scientific literature. The dynamics of such features can have a significant impact on the development of convective storms and, therefore, require much further understanding.

Morcrette et al. (2007) investigated another CSIP case (IOP 1) where a small PV anomaly contributed to the triggering of an isolated convective storm. They also showed how the UM forecasts of that case were very good. Russell et al. (2008) also investigated CSIP IOP 1 but from the perspective of a dry layer of relatively high convective inhibition (CIN) located beneath the small PV anomaly. This dry layer was found to have originated (3 days before the IOP) from the same breaking Rossby wave which gave rise to the small PV anomaly. The case investigated in the present paper (CSIP IOP 9) was very different to IOP 1. Firstly, the PV anomaly was much larger in IOP 9 and the main body of it was not over the UK. Instead, the upper-level influence on the convection in the present investigation arose from a pair of dry layers associated with the tropopause fold of the main PV anomaly and the original streamer. The second significant difference between the two cases was the poor prediction/representation of the storms by the UM during IOP 9. We argue that the complexity and fragmentation of the tropospheric features, together with the precise alignment of the layers with the boundary-layer convergence lines, was responsible for the observed convection. Accurate forecasting of convection in this case would therefore require the model to represent both these processes accurately.

1.3   Aims and paper structure

The aim of this study is to identify the role of an apparently descending dry feature in relation to the initiation and intensification of a band of convective precipitation on 18 July 2005. Figure 1 shows where this precipitation broke out: there were three convective arcs — two over eastern England and one over southern England. This work will concentrate on the latter feature, which occurred in the CSIP experimental area, which was centred on Chilbolton, Hampshire (51.2 °N, 1.4 °W). The origins of the dry feature in question will also be investigated in order to place this event in a wider meteorological context and to help understand similar events that occur in other cases.

The paper is structured as follows. Section 2 introduces the data sources that will be used to meet the aims of this investigation. A synoptic and low-level analysis of the event in question will be presented in Section 3. Section 4 presents specific observations of the apparently descending dry feature and explains why we are referring to them as "apparently" descending. Section 5 identifies the role that the apparently descending dry layers played in forcing the convection and Section 6 examines the way in which this feature arrived over the UK. The importance of these findings will be discussed in Section 7 and conclusions will be drawn in Section 8.

2 Data

The event investigated here occurred on 18 July 2005 during the Convective Storm Initiation Project (CSIP). Observations were taken around Chilbolton (see Fig. 1(a) for the location of places referred to in the text) by a variety of instruments. For more information on the motivation behind CSIP, a more detailed description of the CSIP observational network and brief examinations of some of the major cases of interest, the reader is referred to the project summary by Browning et al. (2007). Here we will specifically present data from: CSIP and UK Met Office radiosondes; CSIP automatic weather stations (AWS); the UK Mesosphere Stratosphere Troposphere (MST) radar (Vaughan, 2002), which is located near Aberystwyth, Wales (52.4 °N, 4.0 °W); European Centre for Medium Range Weather Forecasting (ECMWF) operational analyses; UK Met Office surface synoptic charts; a GPS station; a Radiometrics TP/WVP-3000 microwave radiometer (Ware et al., 2003), which allows retrievals of temperature and humidity profiles with coarse vertical resolution as well as the integrated water vapour and liquid water path; the Total Ozone Mapping Spectrometer (TOMS; Heath et al., 1975); the Meteosat Second Generation (MSG) satellite, specifically Meteosat-8 (Schmetz et al., 2002); the 3 GHz (S-band) Chilbolton Advanced Meteorological Radar, which is known as CAMRa (Goddard et al., 1994); the Universities' Facility for Atmospheric Measurements (UFAM) Aerosol and Ozone LIDAR; and the UFAM UHF wind profiling radar (Norton et al., 2006).

The latter of these instruments — the UHF wind profiling radar — operates at 1290 MHz (23 cm wavelength) with three beams: one pointing to the zenith and two at 17.5° off-vertical. Echoes are obtained from refractive index inhomogenieties in clear air and from raindrops. The turbulent convective boundary layer is full of structure in refractive index and therefore gives a strong echo; layers with sharp gradients in absolute humidity and/or potential temperature (such as are found in atmospheric lids) also show up as layers of enhanced echo power because of the fractal nature (i.e. a cascade of scales) of the gradients. Although the radar only detects sharp layers on a scale of 3 m or less, high-resolution observations show that the stable layers and sharp humidity gradients conventionally revealed by radiosonde profiles (typically hundreds of metres deep) are built up from a myriad of much smaller steps in temperature or humidity (Gage and Green, 1981; Muschinski and Wode, 1998) which together produce the radar echo.

The UK MST radar is a VHF radar, operating at a frequency of 46.5 MHz (wavelength 6.41 m), and is able to observe higher in the atmosphere than the UFAM wind profiler. It is also much less sensitive to precipitation: echo power is due almost entirely to quasi-specular reflection from gradients in static stability and specific humidity (Gage and Green, 1981).

The combination of all these datasets will illustrate the development of a breaking Rossby wave over the Atlantic, the resultant cut-off low (COL) that moved towards the UK and the associated apparently descending double "arm" of relatively high-PV, dry air that helped initiate the convection over the UK.

3 Synoptic and low-level background

Figure 2 shows the synoptic situation for the UK area at 1200 UTC on 18 July 2005. The precipitation event of interest for this investigation was related to the rearmost of two approximately north-south orientated bands of cloud, parts of which were over the UK, as seen in Fig. 2(a). In particular, the two sharp lines of precipitation (maximum rain rate of over 32 mm hr^{-1} at 1645 UTC) that can be seen in Fig. 1(a) coincide with the location of a band of rope cloud seen in the westernmost cloudband in Fig. 2(a). However, the convective elements of this band at 1200 UTC, were very shallow — they were being suppressed by the dry air above. This can be inferred from Fig. 2(b): there was a swathe of dry air over Wales and some of southern England that was covering the area in which the shallow cumulus was observed in Fig. 2(a). This event is similar to that observed by Browning and Roberts (1994), who identified cumulonimbus clouds breaking out at the northern end of rope clouds over the Bay of Biscay under synoptic conditions similar to this case. Indeed, the relatively deep cumulus clouds in our case can be seen in a satellite image from later in the day (Fig. 1(b)) and the convection was observed by CAMRa to reach as high as 5.5 km (Fig. 3). Figure 2(a) also shows the much broader band of cloud associated with the leading SCF, which delivered the light precipitation seen to the east of the narrow lines of intense precipitation in Fig. 1(a).

Figure 2(b) shows the north-south orientated moist (bright) band associated with the leading SCF and, more interestingly, the dry (dark) region over Wales and southern England behind the moist band. As will be seen in Section 6, this feature was rotating eastward (anti-clockwise) around the southern flank of the main "dark eye" (Roberts, 2000) to the north-west of the UK. The "dark eye" is the most obvious feature of Fig. 2(b) and, by comparison with Figs. 2(c) and (d), was clearly related to the tropopause depression (centred on 58°N, 11°W) associated with the cyclone driving the atmospheric circulation in this region. Figure 2(c) also shows an "arm" of relatively high PV (centred about 50°N), which Fig. 2(b) showed was also dry and moving behind the split front (Browning and Monk, 1982) structure that was evident from Fig. 2(a). However, as we will discuss in the remainder of the paper, the westernmost of the SCFs plotted on Fig. 2(c) was related more to the influence of the upper-level features being investigated here rather than any surface features. Finally, Fig. 2(d) shows that the main PV anomaly and the "arm" to the south were coincident with high total ozone measurements and, therefore, correspond to depressions of the tropopause.

Similar to the CSIP case investigated by Morcrette et al. (2007), the convective showers were initiated by a convergence line that was over the southern UK. Evidence for one such convergence line is shown in Fig. 4. Furthermore, data from the array of CSIP automatic weather stations (AWS) and the UFAM wind profiler (neither shown) confirm the view shown in Fig. 4. The wind over the CSIP region was first influenced by the flow around the southern edge of the peninsula, which moved over the CSIP region as south-westerlies. This regime was followed by westerlies deflected to the north of the peninsula — the line where these two flows met represented the convergence line, which moved over the CSIP area at around 1600 UTC. This is typical

of how convergence lines form in this region i.e. downwind of the Devon and Cornwall coasts because of these three methods: the varying effect of land and sea on frictional forces (Hunt et al., 2004), surface temperatures differences between the land and sea (Simpson, 1997) or orographic lifting (Bader et al., 1995). The convergence line provided the boundary layer with the uplift required to overcome the convective inhibition that was present at low-levels. Our focus in this paper, however, is not on the boundary layer forcing but on the much less well understood dynamics responsible for generating potential instability and convective inhibition, and it is to this that we now turn.

4   Observations of the descending dry layers

The observations presented in this case study were taken mostly from stationary, vertically pointing instruments deployed in the UK during the CSIP field campaign. In this section we will discuss the atmospheric features observed from this perspective. Of particular interest in these observations was a pair of dry layers in the troposphere that descended during the day. These layers were observed by several of the CSIP instruments. In the context of the observations, "descending" means that there was a consistent dry layer above the instrument, the height of which decreased with time. This decrease in height occurred because the atmospheric features rotated anti-clockwise and advected horizontally from west to east over the instrument and because of their particular orientation/slope in the atmosphere. In this paper we will refer to this type of descent as *apparent descent* or simply refer to the layer (i.e. not necessarily the air within that layer) descending or sloping. This is in contrast to *physical descent*, which will be used to refer to the vertical motion of a distinct air parcel and has thermodynamic consequences. At this stage of the study we are not stating that the air within this layer had previously descended from upper-levels but that the layer as a whole was descending during the day relative to the instrument observing it i.e. it is the slope of the layer as a whole that is of interest.

To give an example of some of these observations, we can turn to the radiosondes launched from Swanage (50.4 °N, 1.6 °W), which show the feature particularly well (Fig. 5). By examining the red contours — denoting the 10% relative humidity (RH) isoline — it can be seen that there were two distinct dry layers with bases at around 650 and 400 hPa; this double layer structure of the dry region was not evident from Fig. 2. As the two dry layers descended during the day, Fig. 5 (top) shows that the atmospheric column water vapour (WV) measurement also decreased, consistent with dry stratospheric air having intruded into the troposphere.

Figure 5 also shows data from the UFAM UHF radar that was located at Linkenholt (some 85 km to the north east of Swanage). Despite the relatively large distance between Linkenholt and Swanage, the orientation of the leading edge of the descending layer (Figs. 1 and 2(c)) means that it moved over the two locations at approximately the same time. Indeed, the radar detects the moisture gradient at the base of the feature as it moved into its range at around 1615 UTC; coincident with the gradient measured

by the Swanage radiosondes. The radar signal-to-noise ratio (SNR) was also strongly influenced by the precipitation that started at around 1545 UTC. The presence of precipitation is confirmed by the negative vertical wind speeds recorded by the radar (not shown) and the relevant area of the SNR plot appears white in Fig. 5. Furthermore, the radiosondes also show a lid of dry, high-θ_w air at around 850 hPa between 1430 UTC and 1530 UTC, which appears to have had a role in inhibiting the convection until after this time. As will be shown in Fig. 9, this lid was weaker in the region where the convection broke out and, therefore, partially explains why showers were not seen at Swanage. The upper-level features, though, were much more homogeneous over a wider region and, therefore, the Swanage data provides a good illustration of the upper-level features over a wider area.

Figure 6 presents observations from the MST radar and provides a second view of the sloping dry layers over a longer period and up to greater altitudes. The lowermost dry layer can be seen descending from around 8 km (5 UTC) to 3 km (12 UTC) in the MST power return signal (Fig. 6(a)) and the lowest region of this layer also has relatively high vertical shear (Fig. 6(b)). These heights are consistent with Fig. 5 once the distance between Aberystwyth and Linkenholt has been accounted for; the heights of the base of these two layers as measured by the radiosondes have been plotted over the MST data but it should be noted that these layers can be traced beyond the radiosonde measurements in the MST data. The uppermost dry layer is less clearly defined in the power signal but appears to start from approximately the same point as the lower layer and only descends to 4 km by 1530 UTC. The region of low return signal power between 0700 and 0800 UTC and 2 to 3 km is an indicator of the frontal rain that passed over Aberystwyth (see Fig. 1(a)) at this time and then moved on to the CSIP area.

The impact of the lowermost dry layer can also be seen in observations made by the UFAM Ozone and Aerosol LIDAR (located at Chilbolton) as the layer reached its lowest point — down to as low as 1.8 km — after around 1800 UTC (Fig. 7), which is consistent with radiosondes launched from Chilbolton at this time (not shown). The low aerosol backscatter co-efficient region above around 1.75 km shows where the apparently descending dry layer met the high aerosol backscatter co-efficient region i.e. the boundary layer. There was no signal from the LIDAR before this time due to the extensive cloud cover at Chilbolton but even this observation from later in the day helps to identify the role of the feature.

Figure 8 also shows the apparent descent of dry air over the CSIP region, this time from radiometer data. The passing of the storm and the associated precipitation can also be seen as the vertical peak in RH at around 1600 UTC. What is also interesting here is the reduced depth of the surface moist layer beneath the descending dry air. This will be discussed further in the next section as it was another key factor in the development of the convection. This reduction had the important effect of amplifying the changes in surface moisture, which altered from dry (0900 to 1300 UTC) to moist (1300 to 1800 UTC). This change was also observed by the Advanced Clear-air Radar for Observing the Boundary layer And Troposphere (ACROBAT; data not shown), which is a UHF radar mounted on the same Chilbolton dish as CAMRa.

All the observations of the dry layers presented in this section show them apparently descending. This is not what would be expected from the synoptic data presented in Fig. 2, which showed a cold front moving from west to east over the UK. This would normally be observed as a layer ascending with time over a fixed point; descent with time normally characterises a warm front (Bjerknes and Solberg, 1922). The explanation for this contradiction lies in the way that the rotation around the depression to the north-west of the UK altered how the CSIP instruments observed the features. Whilst this will be investigated further in Section 6, it has been noted here to avoid confusion that could otherwise arise from these observations.

In this section we have identified the dry feature in question, shown that it had two distinct layers emanating from a tropopause depression and that the origin/nature of the feature requires some more investigation to understand it fully. It is now necessary to analyse the impact of these apparently descending layers on the convective stability of the troposphere during this case.

5   Convective stability of the troposphere

The potential temperature (θ) profiles from the Swanage soundings (not shown) showed no evidence of a depressed tropopause or an upward curvature of the isentropes in the troposphere. This was typical of all the locations where radiosondes were launched during this case (i.e. Reading (51.4 °N, 1.0 °W), Chilbolton, Bath (51.4 °N, 2.4 °W) and Larkhill (51.2 °N, 1.8 °W)). Therefore, it can be assumed that the method by which upper-level PV anomalies often influence convection, as discussed in the Section 1, was not at work in this case. Indeed, the main body of the PV anomaly (Fig. 2(c)) was too far north to influence the tropospheric stability in this way over southern Britain — this case was driven more by what occurred at the fringes of the PV anomaly.

Figure 9, however, shows how the change in the surface and mid-tropospheric conditions above Larkhill and Reading between 1200 and 1600 UTC helped create the conditions that led to the convective showers. The relative dryness in the surface layer at 1200 UTC (Fig. 9(a)) resulted in the lifted surface parcel being limited by the base of a strong inversion, or lid, at around 850 hPa. However, by 1600 UTC at Reading the surface layer had moistened due to the moisture convergence forced by the low-level flow examined in Fig. 4, which was initially capped by the apparent descent of dry air from above (Fig. 8). The dry layer had also reached Reading by 1600 UTC and Fig. 5 shows a decrease in θ_w with height above 850 hPa (i.e. potential instability — dry, low θ_w air above moist, high θ_w air) coincident with the arrival of the leading edge of the dry layer. This, as will be shown later in this section, increased the convective available potential energy (CAPE) in the mid-troposphere.

However, and perhaps more importantly, Fig. 9(b) shows that the temperature profile between about 925 and 450 hPa mostly stays to the left of the moist adiabat associated with the lifted surface parcel, indicating that it is unstable (i.e. convective instability). The fact that the lifted surface parcel does not clear the lid at 650 hPa highlights the intricate interplay of the features forcing the convection

during this case and that the window of opportunity for convection to develop was short. (The aforementioned lid at 650 hPa can be seen in Fig. 3 as the approximately horizontal layer at around 3 km extending from the convective plumes.)

The key point is that the convection could only develop at the point where the surface moisture convergence coincided with weak convective inhibition combined with potential instability — this is very nearly the case in Fig. 9(b). We interpret this finding as follows: at the leading edge of a dry layer the air is of upper tropospheric origin with low relative humidity but not much static stability. In the main body of the layer, air from the tropopause region is found, whose elevated PV manifests itself as enhanced static stability rather than absolute vorticity due to the vertical extent of the anomaly. This increase in static stability provides convective inhibition (CIN) beneath the main body of the descending layer; the cooling of the boundary layer also reduces the mid-tropospheric CIN. There was only a short period of time when all these conditions were met and, thus, the band of showers was narrow.

The lowermost descending dry layer appears to have played a further role in initiating the convection by introducing colder air directly below it, which resulted in the weakening of the lid that was previously seen at 725 hPa (Fig. 9(a)). Had this lid persisted until the 1600 UTC Reading sounding (Fig. 9(b)) it would have very likely capped the convection at that height. Hill and Browning (1987) have previously described how this cooling mechanism affects atmospheric stability.

These profiles (Fig. 9) can also be used to assess the relative importance of the surface changes (i.e. moistening and cooling) and mid-tropospheric changes (i.e. the descent of the dry layers leading to the potential instability) throughout the day. To do this, the changes in convective available potential energy (CAPE) from the Larkhill 1158 UTC to the Reading 1605 UTC sounding have been attributed to one or other of the two processes. CAPE is calculated using the method described by Emanuel (1994). Firstly, the surface parcel of the Larkhill 1158 UTC sounding was moistened and cooled to the level of the Reading 1605 UTC sounding. Calculating the CAPE of this new surface parcel increased the CAPE of the Larkhill 1158 UTC profile by 117 J kg^{-1}. This essentially quantifies the impact on CAPE that the moistening and cooling that occurred between the two profiles had. The CAPE value of the surface parcel of the unmodified Reading 1605 UTC sounding was 325 J kg^{-1}. The difference between this value and the CAPE of the modified Larkhill 1158 UTC is 153 J kg^{-1}. This value represents the impact on CAPE that the potential instability had as it is the only significant difference between the modified Larkhill 1158 UTC profile and the unmodified Reading 1605 UTC sounding. From this analysis it can be stated that the changes in the upper- and mid-levels during the day had the greater impact on CAPE than the boundary layer changes (117 vs. 153 J kg^{-1}). However, it must not be forgotten that it was the convergence line that triggered the convection so both were essential in the development of the storms.

As discussed in the previous section, in relation to Fig. 8, it can also be seen that the apparent descent of dry stable air to such low levels played a role in amplifying the impact of the convergence line; in limiting the vertical extent of the boundary layer, the apparently descending dry air al-

lowed the RH to increase to such an extent as to promote the likelihood of deep convection. This increase in low-level RH can be inferred from the radiosonde ascents in Fig. 9 and seen directly in the radiometer data in Fig. 8, which also shows the lower portion of the dry layer (with the same shape as seen in Fig. 5 from 6 km at 1200 UTC to 4 km at 1500 UTC) limiting the vertical extent of the moist region. There was also a dry region near the surface which can be seen in Fig. 8 between 0900 and 1300 UTC and up to 1300 UTC in Fig. 5 — low radar echo power signifies dry air. This initial dryness would have delayed the onset of convection.

Figure 9(b) also indicates that, once the lids had been breached, convection was free to reach around 450 hPa, which was around the same height that the convection was seen to reach by the Chilbolton radar (Fig. 3). Interestingly, Fig. 9(b) also shows that it was the upper-most dry layer that was responsible for halting the convection at 450 hPa, meaning that the dry feature, as a whole, contributed both to the convective initiation and, subsequently, to limiting its vertical extent. This is a similar role to that played by the resultant parts of a breaking Rossby wave investigated by Russell et al. (2008) from CSIP IOP 1 (15 June 2005). In that case, however, the lid was located beneath an upper-level PV anomaly (not between the tropopause and a lower level PV anomaly as seen here), and was responsible for the widespread convective inhibition seen in that case.

To extend the CSIP observations and place them in context, we now present diagnostics from the ECMWF operational analyses for this day. Figure 10 shows a cross section of RH and temperature along the dashed line shown in Fig. 2(c), NW-SE from Iceland to Brest. This, like the observations, shows a moist boundary layer beneath a sloping dry region (which consists of two dry layers, see Fig. 5) southeastward of 10°W. Figure 11(a) shows the corresponding PV cross section, seemingly identifying the dry layers as extrusions of tropopause level air from the tropopause depression centred around 12°W. In Section 6 we will show that this view is too simplistic but it is useful to continue with this interpretation at this point while noting the complexity of the PV anomaly.

Browning (1997) showed how the driest region of an intrusion coincides with the region of maximum overrunning; this is also the case here. Similarly, we can see, by considering both Figs. 10 and 11(a), that the sloping region of high PV (if viewed as a single feature rather than two distinct layers) is slicing into a region of relatively high RH i.e. the moist surface layer beneath the intrusion and the relatively high RH column at around 5°W that reaches up to around 200 hPa. This also agrees with the overrunning θ_w surfaces mechanism summarised by Browning (1997) and we can, therefore, be more confident in one of our hypotheses regarding the mechanisms by which the convection was induced in the present case.

In itself the reporting of two sloping dry layers of this sort is rare, especially as they were observed, to some extent, by the radiosondes, MST radar, the UFAM wind profiling radar and the UFAM LIDAR. The features were also well captured by the ECMWF operational model which is in good agreement with our observations. These layers were also partly responsible for inducing deep convection and then inhibiting the convection at a higher level, which makes this a very interesting case. How these features developed in the wider synoptic context remains to be seen. It is to this that we now turn.

6   Development of the cut-off low and the sloping dry layers

So far in this study we have concentrated on the role of the sloping dry layers in forcing the convection observed on 18 July 2005. In order to understand the importance of this event we need to understand how the situation arose. With this in mind, Fig. 12 shows a PV perspective of the build up to the convective showers over the UK. Similar to the situation from CSIP IOP 1 (Russell et al., 2008), the event was preceded by a breaking Rossby wave (second life-cycle category (LC2) of Thorncroft et al. (1993)) over the Atlantic in the present case. This case differs from IOP 1 in that the wave broke much further north over the Atlantic. By 0000 UTC on 17 July 2005, a cut-off low had formed at around 60°N, 25°W and was rotating and slowly moving south–eastwards towards the UK. As a fold started to develop in the baroclinic region to the west of the PV anomaly, upper-level air was drawn around the fringes of the main body of the feature (best seen in Figs. 12 and 2(c)). Subsequently, this flow apparently descended over the UK due to the influence of the PV anomaly on the isentropes (see Fig. 11) and was also drawn eastwards as a result of the cyclonic rotation of the PV anomaly.

Figure 11 gives a vertical perspective of the PV anomaly. Whilst Fig. 11(a) shows the two layers very well, it does not explain why they were observed to slope in the way that they were. How did this occur? In short, it was the rotation around the PV anomaly that was critical to the development and morphology of the two dry layers. By plotting a further vertical cross-section of PV around the depression (Fig. 11(b); see Fig. 12(f) for the path of this cross-section) we can see how regions of high PV were pulled anti-clockwise (cyclonically) around the depression from what remained of the original streamer to the west of the COL. This caused the streamer to fragment and where these fragments reached the eastern side of the depression (where there was a small fold, which was observed as the lowermost dry layer) they were observed as the higher of the dry layers. Examples of these fragments can be identified on Fig. 11(b) at 700 hPa between points 17 and 20 and, more significantly, at 400 hPa between points 20 and 30. The latter of these eventually formed the uppermost dry layer.

As well as the twisting, the rotation also partially explains why the frontal surfaces were observed to descend with time in the CSIP area, when a cold frontal surface observed at a fixed location would normally ascend with time as a weather system moved across that point (Bjerknes and Solberg, 1922). The fact that the structure as a whole sloped in the north-south direction — it was higher in the north than the south — provides the rest of the explanation. Initially, the MST radar and radiosondes would have been on the south-eastern fringe of the folded structure associated with the PV anomaly, where the fold was at a greater elevation than at the southern edge. As the day progressed, the PV anomaly rotated cyclonically, which moved the lower regions of the fold (and the fragment) over the southern UK. This rotation gave the impression in the observations

that the layers were descending. However, the layers were ascending radially towards the centre of the PV anomaly, as Fig. 11(a) shows. If the feature were observed along its radius, as in Fig. 11(a), then apparent ascent would have been observed. This explanation is relatively complicated so we have simplified this description in a schematic sketch in Fig. 13 that summarises this mechanism.

7   Discussion and representation of convection in the Met Office mesoscale Unified Model

As introduced in Section 1, the UK Met Office Unified Model (UM) was run for this case at various resolutions, all of which fell short in capturing the details of the showers. As well as the then operational 12 km resolution mesoscale model, the UM was also run quasi-operationally at 4 km resolution and in a post event trial mode at 1 km resolution in a limited domain over the CSIP area (see Clark and Lean, 2006, for more details). Whilst the UM at these various resolutions captures the intensity and orientation of the frontal precipitation quite well, none of these models adequately capture the extent, consistency or orientation of the line of showers behind the front, as seen in figure 50 of Clark and Lean (2006). The differences between these precipitation forecasts and the observations can be summarised thus:

• The angle of the line appears good in the 12 km resolution model but the intensity is too low and neither of the regions of precipitation associated with the front or the line of showers are continuous enough.

• The 4 km model produces a very intense oval of precipitation approximately perpendicular (rather than parallel) to the front, which is also represented as more intense than the rainfall radar observed.

• Finally, the 1 km model produces the most continuous line of showers when compared with the other two runs but it is too intense and at the wrong angle when compared to the radar observations.

This implies that the UM has not represented the complex structure of the angle of the leading edge of the dry intrusion adequately or its interaction with the surface convergence line. The overestimation of the intensity in the model was due to poor representation of the uppermost dry layer in the model (Peter Clark, personal communication). We have shown in Fig. 9 that this layer was ultimately responsible for capping the convection in this case but, in the model, it was not dry or warm enough relative to its environment to cap the convection at around 450 hPa as observed.

As far as we are aware, they are no other observations of double apparently descending layers in the meteorological literature. From this analysis, it appears to be derived from a PV anomaly with a strong cyclonic rotation. The climatological occurrence of such events is unknown and requires further investigation. This would be a potentially significant study to undertake as the simultaneous passing of two dry layers influences the intensity of the convection observed and, as discussed above, is not well represented by mesoscale models such as the UM.

More generally, this case highlights the importance of sloping layers in both promoting convection via the reduction in tropospheric stability and the weakening of lids as well as their role in capping convection once it has been initiated.

8   Conclusions

On 18 July 2005, two sloping dry layers passed over the UK at around 800 and 500 hPa whilst, nearer the surface, a narrow band of convective showers developed behind a pair of cold fronts with the aid of a surface convergence line. The lowermost of these layers (a tropopause fold on the eastern side of the depression) helped to promote these showers by reducing the tropospheric stability by introducing potential instability and by weakening a lid that had previously been capping the convective development. Furthermore, once the convection was initiated, the uppermost dry layer (a fragment of the streamer on the western side of the depression, drawn around the depression in the cyclonic rotation) capped the convection at around 450 hPa. The period when convection was possible was very short as it required all the factors at work — the convergence line/surface moisture, adequate surface temperature, increase in mid-tropospheric CAPE and decrease in mid-tropospheric CIN — to all coincide, this explains the narrowness of the shower band. It was also shown that whilst the convergence line triggered the convection it was the potential instability that had the greater impact on the convective available potential energy (CAPE). This case was intensively observed during the Convective Storm Initiation Project (CSIP) and some of these measurements have been used to investigate the role and origin of these features.

9   Acknowledgements

REFERENCES

Bader, M. J., Forbes, G. S., Grant, J. R., Lilley, R. B. E. and Waters, A. J., 1995. *Images in weather forecasting: a practical guide for interpreting satellite and radar imagery*. Cambridge University Press, 499 pp.

Bennett, L. J., Browning, K. A., Blyth, A. M., Parker, D. J. and Clark, P. A., 2006. A review of the initiation of precipitating convection in the United Kingdon. *Q. J. R. Meteorol. Soc.* **132**, 1001–1020.

Bjerknes, J. and Solberg, H., 1922. Life cycle of cyclones and the polar front theory of atmospheric circulation. *Geophys. Publ.* **3**, 1–18.

Browning, K. A., 1997. The dry intrusion perspective of extra-tropical cyclone development. *Meteorol. Appl.* **4**, 317–324.

Browning, K. A. and Monk, G. A., 1982. A simple model for the synoptic analysis of cold fronts. *Q. J. R. Meteorol. Soc.* **108**, 435–452.

Browning, K. A. and Roberts, N. M., 1994. Use of satellite imagery to diagnose events leading to frontal thunderstorms: part I of a case study. *Meteorol. Appl.* **1**, 303–310.

Browning, K. A. and Roberts, N. M., 1995. Use of satellite imagery to diagnose events leading to frontal thunderstorms: part II of a case study. *Meteorol. Appl.* **2**, 3–9.

Browning, K. A., Blyth, A. M., Clark, P. A., Corsmeier, U., Morcrette, C. J. and co-authors, 2007. The Convective Storm Initiation Project. *Bull. Am. Meteorol. Soc.* **88**, 1939–1955.

Clark, P. A. and Lean, H., 2006. An overview of high resolution UM performance for CSIP cases. *JCMM Internal Report, No. 155* 42pp.

Cullen, M. J. P., 1993. The unified forecast/climate model. *Meteorol. Mag.* **122**, 81–94.

Danielsen, E. F., 1964. Project Springfield Report. Defense Atomic Support Agency, 20301, DASA 1517(NTIS#AD-607980), Washington D. C., 99pp.

Danielsen, E. F., 1968. Stratospheric-troposheric exchange based on radioactivity, ozone and potential vorticity. *J. Atmos. Sci.* **25**, 502–518.

Emanuel, K. A., 1994. *Atmospheric Convection*. Oxford University Press, 580 pp.

Gage, K. S. and Green, J. A., 1981. Evidence for specular reflection from monostatic VHF radar observations of the stratosphere. *Radio Sci.* **13**, 991–1001.

Goddard, J. W. F., Eastment, J. D. and Thurai, M., 1994. The Chilbolton Advanced Meteorological Radar: A tool for multidisciplinary atmospheric research. *Electron. Commun. Eng. J.* **6**, 77–86.

Golding, B., 1998. Nimrod: A system for generating automated very short range forecasts. *Meteorol. Appl.* **5**, 1–16.

Golding, B., Clark, P. A. and May, B., 2005. The Boscastle flood: Meteorological analysis of the conditions leading to flooding on 16 August 2004. *Weather* **60**, 230–235.

Griffiths, M., Thorpe, A. J. and Browning, K. A., 2000. Convective destabilization by a tropopause fold diagnosed using potential-vorticity inversion. *Q. J. R. Meteorol. Soc.* **126**, 125–144.

Heath, D. F., Krueger, A. J., Roeder, H. A. and Henderson, B. D., 1975. The solar back-scatter ultraviolet and total ozone mapping spectrometer (SBUV/ TOMS) for Nimbus G. *Opt. Eng.* **14**, 323–331.

Hill, F. F. and Browning, K. A., 1987. Case study of a persistent mesoscale cold pool. *Meteorol. Mag.* **116**, 297–309.

Hoskins, B. J., McIntyre, E. M. and Robertson, A. W., 1985. On the use and significance of isentropic potential vorticity maps. *Q. J. R. Meteorol. Soc.* **111**, 877–946.

Hunt, J. C. R., Orr, A., Rottman, J. W. and Capon, R., 2004. Coriolis effects in mesoscale flows with sharp changes in surface conditions. *Q. J. R. Meteorol. Soc.* **130**, 2703–2731.

Marsham, J. H. and Parker, D. J., 2006. Secondary iniation of multiple bands of cumulonimbus over southern Britain. Part II: Dynamics of secondary initiation. *Q. J. R. Meteorol. Soc.* **132**, 1053–1072.

Marsham, J. H., Morcrette, C. J., Browning, K. A., Blyth, A. M., Parker, D. J., Corsmeier, U., Kalthoff, N. and Kohler, M.,

2007a. Variable cirrus shading during CSIP IOP 5. I: Effects on the initiation of convection. *Q. J. R. Meteorol. Soc.* **133**, 1643–1660.

Marsham, J. H., Blyth, A. M., Parker, D. J., Beswick, K., Browning, K. A., Corsmeier, U., Kalthoff, N., Khodayar, S., Morcrette, C. J. and Norton, E. G., 2007b. Variable cirrus shading during CSIP IOP 5. II: Effects on the convective boundary layer. *Q. J. R. Meteorol. Soc.* **133**, 1661–1675.

Morcrette, C. J., Browning, K. A., Blyth, A. M., Bozier, K. E., Clark, P. A., Ladd, D., Norton, E. G. and Pavelin, E., 2006. Secondary iniation of multiple bands of cumulonimbus over southern Britain. Part I: An observational case study. *Q. J. R. Meteorol. Soc.* **132**, 1021–1051.

Morcrette, C. J., Lean, H., Browning, K. A., Roberts, N., Clark, P. A., Nicol, J., Russell, A. and Blyth, A. M., 2007. Combination of mesoscale and synoptic mechanisms for triggering of an isolated thunderstorm: a case study of CSIP IOP 1. *Mon. Wea. Rev.* 3728–3749.

Muschinski, A. and Wode, C., 1998. First in situ evidence for coexisting submeter temperature and humidity sheets in the lower free troposphere. *J. Atmos. Sci.* **55**, 2893–2906.

Norton, E. G., Vaughan, G., Methven, J., Coe, H., Brooks, B., Gallagher, M. and Longley, I., 2006. Boundary layer structure and decoupling from synoptic scale flow during NAMBLEX. *Atmos. Chem. Phys.* **6**, 433–445.

Roberts, N. M., 2000. The relationship between water vapour imagery and thunderstorms. *JCMM Internal Report, No. 110* 40pp.

Russell, A., Vaughan, G., Norton, E. G., Morcrette, C. J., Browning, K. A. and Blyth, A. M., 2008. Convective inhibition beneath an upper-level PV anomaly. *Q. J. R. Meteorol. Soc.* **134**, 371–383.

Schmetz, J., Pili, P., Tjemkes, S., Just, D., Kerkmann, J., Rota, S. and Ratier, A., 2002. An introduction to Meteosat Second Generation (MSG). *Bull. Am. Meteorol. Soc.* **83**, 977–992.

Simpson, J. E., 1997. *Gravity currents in the environment and the laboratory 2nd edition*. Cambridge University Press, 244 pp.

Thorncroft, C. D., Hoskins, B. J. and McIntyre, E. M., 1993. Two paradigms of baroclinic-wave life cycle behaviour. *Q. J. R. Meteorol. Soc.* **119**, 17–55.

Vaughan, G., 2002. The UK MST radar. *Weather* **57**, 67–73.

Vaughan, G., Price, J. D. and Howells, A., 1994. Transport into the troposphere in a tropopause fold. *Q. J. R. Meteorol. Soc.* **120**, 1085–1103.

Ware, R., Solheim, F., Carpenter, R., Gueldner, J., Liljegren, J., Nehrkorn, T. and Vandenberghe, F., 2003. A multi-channel radiometric profiler of temperature, humidity and cloud liquid. *Radio Sci.*, **38**, 8079–8092.

Figure Captions

Figure 1. The convective showers being investigated in this paper as represented by: a) the rainfall radar network, showing the precipitation rate at 1615 UTC on 18 July 2005; and b) high-resolution visible imagery from the Meteosat-8 satellite at 1615 UTC showing the cloudbands relating to the rainfall shown in Fig. 1(a). The locations of places referred to in the text are also shown on Fig. 1(a).

Figure 2. Summary of the conditions over the UK at 1200 UTC on 18 July 2005: a) high-resolution visible image from Meteosat-8 showing the cloud bands associated with the two cold fronts shown in Fig. 2(c); b) contrast enhanced water vapour (WV) image from Meteosat-8 showing the dry regions relating to the PV anomaly located to the north-west of the UK and the dry "arm" over the southern UK; c) ECMWF operational analysis of potential vorticity (PV) in PV units (PVU; i.e. 1.0×10^{-6} m^2 s^{-1} K kg^{-1}) on the 315 K isentropic surface (see Fig. 11(a) for the height of this surface) with the UK Met Office frontal analysis for 1200 UTC superimposed; and d) total ozone (in Dobson Units; DU) at ∼1130 UTC from TOMS, contours are every 20 DU. The TOMS data are indicative of the tropopause depression associated with the PV anomaly as the total ozone column detected by the spectrometer is enhanced by the intrusion of stratospheric, high-ozone air to lower levels than usual as the PV anomaly results in the stretching of the vortex into the upper-troposphere. Darker shading indicates higher levels of PV and O$_3$ for Figs. 2(c) and (d), respectively. The dashed line plotted on Fig. 2(c) represents the line through which the vertical cross sections presented in Figs. 10 and 11(a) are plotted.

Figure 3. Range-height indicator (RHI) of reflectivity (dBZ) from the 3 GHz radar (CAMRa) located at Chilbolton (51.2 °N, 1.4 °W). This RHI was taken at 1459 UTC and was at an azimuth of 270° to the north.

Figure 4. 10 m winds (scaled arrows) and convergence (shading) from NIMROD i.e. the Met Office nowcasting model (Golding, 1998). The location of Chilbolton is marked by a blue cross.

Figure 5. The main line-contour plot shows: wet-bulb potential temperature (θ_w; solid lines; contour interval is 1 K); the < 10% relative humidity (RH) area (grey shading, where there is no overlap with the radar data, darker = lower RH); the 10% RH contour (red lines) and; the lifting condensation level (LCL; thick black dashed line) all from the Swanage soundings for 18 July 2005. The vertical lines at the top of the profile indicate the radiosonde release times and the contours have been interpolated from this data. The colour plot between 995 and 630 hPa shows signal to noise ratio recorded, in dBZ, from the UFAM wind profiling radar that was located at Linkenholt. The smaller top plot shows atmospheric WV derived from a GPS station at Linkenholt. The text in the box at the bottom of the figure describes the conditions as recorded by a web-camera located by the wind profiler at Linkenholt (51.3 °N, 1.5 °W).

Figure 6. Data from the MST radar (located at Aberystwyth) for 18 July 2005 showing the period 0300–2100 UTC for: a) radar return signal power (dBZ) below

10 km ; and b) vertical shear (ms^{-1} km^{-1}) below 7 km. Vertical shear is equal to du/dz calculated between radar gates (300 m). The vertical extent of the vertical shear plot has been limited to 7 km as there are very high values in the stratosphere that are not relevant to our investigation. The dashed black and white lines indicate the height of the bases of the two dry layers as identified by the Swanage radiosondes (Fig. 5) with the distance between Aberystwyth and Swanage accounted for.

Figure 7. Aerosol backscatter co-efficient (β) from the 355 nm beam of the UFAM Ozone and Aerosol Lidar. The darkest reds correspond to areas of cloud whereas the light blue, green and yellow areas show regions of aerosol in the boundary layer. The dark blue and white regions show the clean air that was apparently descending overhead during the day and suppressing the boundary layer growth.

Figure 8. Vertical RH (%) profile from a UK Met Office Radiometrics TP/WVP-3000 microwave radiometer that was located at Linkenholt. The dashed black and white line indicates the height of the base of the lowermost dry layer as identified by the Swanage radiosondes (Fig. 5).

Figure 9. Dry bulb temperature (T; solid line) and dew-point temperature (T_d; dot-dashed line) measured by radiosondes launched from: a) Larkhill at 1158 UTC; and b) Reading at 1605 UTC. The lifting condensation level (LCL) has been plotted onto these soundings (i.e. where the solid grey lines starting from the surface T and T_d meet when, respectively, the dry adiabat and the line of constant mixing ratio are followed upwards) and, in the case of Fig. 9(b), the vertical parcel trajectory (dashed grey line) has been continued from the LCL up the moist adiabat to show that the surface parcel would have reached about 450 hPa. It should also be noted that as a result of the irregular radiosonde launch times during this IOP, we are not able to illustrate the two phases of this case using soundings from the same location. However, Larkhill and Reading are relatively close (see Fig. 1) and would be influenced by the same surface and upper-level conditions due to the eastward flow of the major features being investigated here.

Figure 10. Relative humidity (RH; shading) and temperature (°C; white contours with an interval of 4°C) from the ECMWF operational analyses at 1200 UTC on 18 July 2005. This plot is a cross section through the dashed line seen in Fig. 2(c) i.e. from 20°W, 64°N to 2°W, 46°N.

Figure 11. PV (in PVU; solid contours and shading; contour interval is 0.25 PVU below 2 PVU, and 1 PVU above 2 PVU; and darker shading relates to higher PV) and potential temperature (θ; dashed contours; contour interval is 15 K) from the ECMWF operational analyses at 1200 UTC for Figs. 11(a) and 0600 UTC for Fig. 11(b) on 18 July 2005. These data are plotted as cross sections through: a) the dashed line seen in Fig. 2(c) i.e. from 20°W, 64°N to 2°W, 46°N; and b) along the curved path shown by the circular points plotted on Fig. 12(f).

Figure 12. A selection of ECMWF operational analyses of PV (thick contours and shading) on the 315 K isentropic surface for the build up to the descending layers of upper-level air moving over the UK on the 18 July 2005.

The contour interval is 1 PVU (i.e. 1.0×10^{-6} m^2 s^{-1} K kg^{-1}) and darker regions of shading show areas of higher PV. ECMWF operational analyses mean sea-level pressure (MSLP) is also plotted here (dotted contours; contour interval is 5 hPa; dash-dotted contour, for reference, is the 1020 hPa isobar). The position of relevant fronts (there were other fronts present for each time shown) from the Met Office surface analyses are plotted as well. The dots plotted on Fig. 12(f) relate to the grid points used to plot the vertical PV cross-section shown in Fig. 11(d). Point number (as used on the x-xaxis of Fig. 11(d)) increases from 0 in the north-west to 36 in the south-east. Points 10, 20 and 30 can be identified by being bigger than the other points and they have a cross plotted on them.

Figure 13. Schematic of a PV isosurface (approximately 1 PVU) based on the evidence presented in this paper. The schematic represents the tropospheric PV structure at approximately 0000 UTC on 18 July 2005 — a sketch of mainland Britain has been included to indicate the scale and location the the PV isosurface. Elevated features are shaded dark grey and the ground is shaded light grey. The sloping round/annular shaped feature in the centre of the drawing shows the downward flow in the upper-troposphere from the base of the main PV anomaly. The base of the round feature was higher in the north than in the south; this is indicated by the dotted lines (vertical and horizontal) that show how the features would translate onto the ground. The arrows indicate that the round feature was moving eastwards and rotating anti-clockwise but, because of the north to south slope, it was precessing around a moving axis rather than around a fixed vertical axis. Under these circumstances, observations taken from a fixed point beneath the round feature would show that it's base reduced in height over time. The points A and B plotted on Fig. 13 represent two such observations taken in the frame of reference stationary with respect to the rotating feature; this shows how an observer would see the base coming down in height, as was seen in this case. The streamer to the west of the main PV "skirt" has been plotted to show the source of the upper-most PV fragment that was observed during the case.
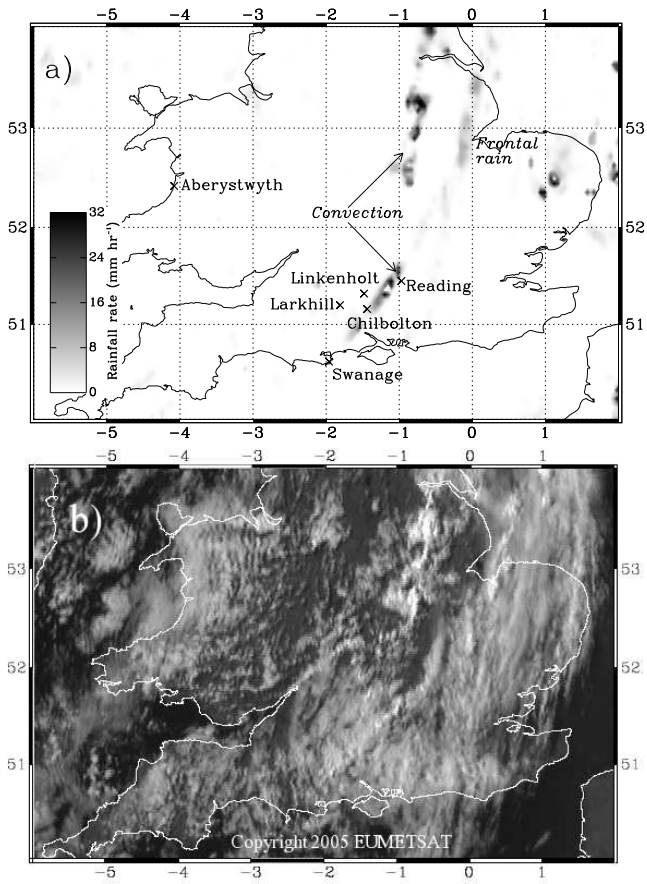
Figure 1. The convective showers being investigated in this paper as represented by: a) the rainfall radar network, showing the precipitation rate at 1615 UTC on 18 July 2005; and b) high-resolution visible imagery from the Meteosat-8 satellite at 1615 UTC showing the cloudbands relating to the rainfall shown in Fig. 1(a). The locations of places referred to in the text are also shown on Fig. 1(a).
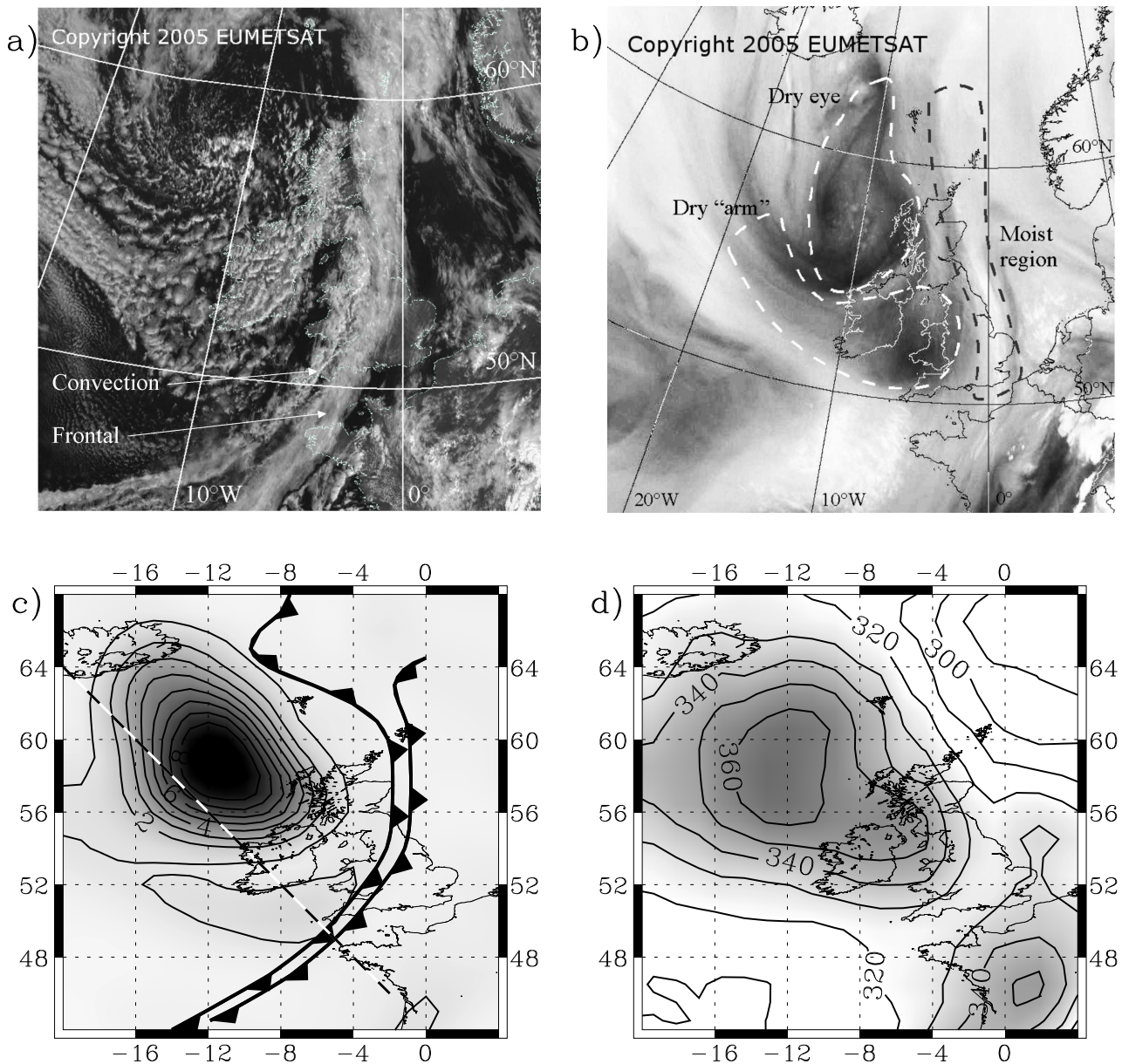
Figure 2. Summary of the conditions over the UK at 1200 UTC on 18 July 2005: a) high-resolution visible image from Meteosat-8 showing the cloud bands associated with the two cold fronts shown in Fig. 2(c); b) contrast enhanced water vapour (WV) image from Meteosat-8 showing the dry regions relating to the PV anomaly located to the north-west of the UK and the dry "arm" over the southern UK; c) ECMWF operational analysis of potential vorticity (PV) in PV units (PVU; i.e. 1.0×10^{-6} m^2 s^{-1} K kg^{-1}) on the 315 K isentropic surface (see Fig. 11(a) for the height of this surface) with the UK Met Office frontal analysis for 1200 UTC superimposed; and d) total ozone (in Dobson Units; DU) at ~1130 UTC from TOMS, contours are every 20 DU. The TOMS data are indicative of the tropopause depression associated with the PV anomaly as the total ozone column detected by the spectrometer is enhanced by the intrusion of stratospheric, high-ozone air to lower levels than usual as the PV anomaly results in the stretching of the vortex into the upper-troposphere. Darker shading indicates higher levels of PV and O$_3$ for Figs. 2(c) and (d), respectively. The dashed line plotted on Fig. 2(c) represents the line through which the vertical cross sections presented in Figs. 10 and 11(a) are plotted.

Figure 3. Range-height indicator (RHI) of reflectivity (dBZ) from the 3 GHz radar (CAMRa) located at Chilbolton (51.2 °N, 1.4 °W). This RHI was taken at 1459 UTC and was at an azimuth of 270° to the north.
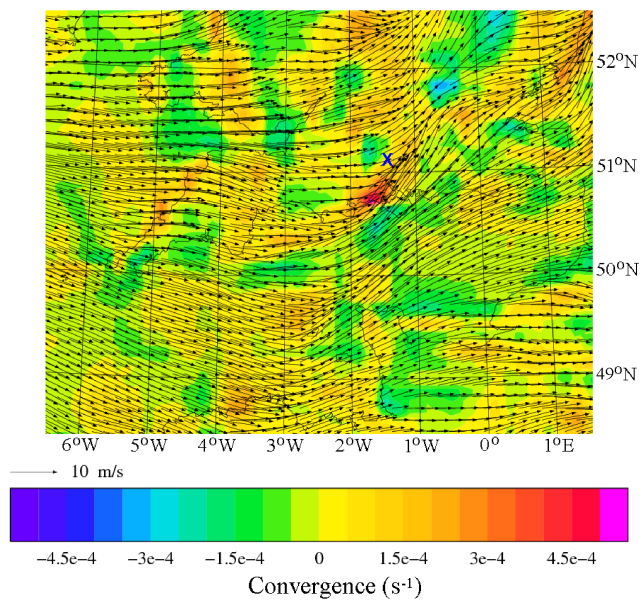
Figure 4. 10 m winds (scaled arrows) and convergence (shading) from NIMROD i.e. the Met Office nowcasting model (Golding, 1998). The location of Chilbolton is marked by a blue cross.
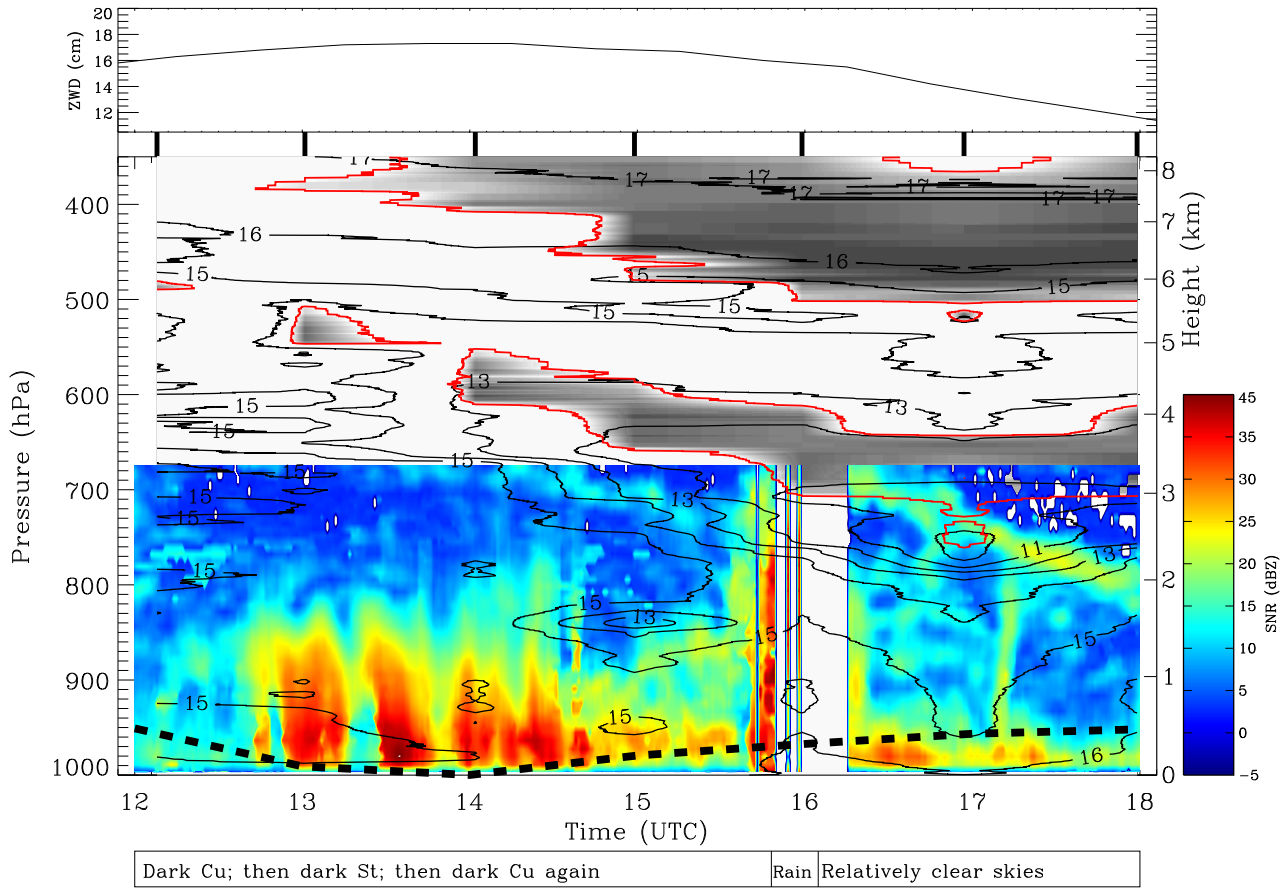
Figure 5. The main line-contour plot shows: wet-bulb potential temperature (θ_w; solid lines; contour interval is 1 K); the $< 10\%$ relative humidity (RH) area (grey shading, where there is no overlap with the radar data, darker = lower RH); the 10% RH contour (red lines) and; the lifting condensation level (LCL; thick black dashed line) all from the Swanage soundings for 18 July 2005. The vertical lines at the top of the profile indicate the radiosonde release times and the contours have been interpolated from this data. The colour plot between 995 and 630 hPa shows signal to noise ratio recorded, in dBZ, from the UFAM wind profiling radar that was located at Linkenholt. The smaller top plot shows atmospheric WV derived from a GPS station at Linkenholt. The text in the box at the bottom of the figure describes the conditions as recorded by a web-camera located by the wind profiler at Linkenholt (51.3 °N, 1.5 °W).

Figure 6. Data from the MST radar (located at Aberystwyth) for 18 July 2005 showing the period 0300–2100 UTC for: a) radar return signal power (dBZ) below 10 km ; and b) vertical shear (ms^{-1} km^{-1}) below 7 km. Vertical shear is equal to du/dz calculated between radar gates (300 m). The vertical extent of the vertical shear plot has been limited to 7 km as there are very high values in the stratosphere that are not relevant to our investigation. The dashed black and white lines indicate the height of the bases of the two dry layers as identified by the Swanage radiosondes (Fig. 5) with the distance between Aberystwyth and Swanage accounted for.

Figure 7. Aerosol backscatter co-efficient (β) from the 355 nm beam of the UFAM Ozone and Aerosol Lidar. The darkest reds correspond to areas of cloud whereas the light blue, green and yellow areas show regions of aerosol in the boundary layer. The dark blue and white regions show the clean air that was apparently descending overhead during the day and suppressing the boundary layer growth.
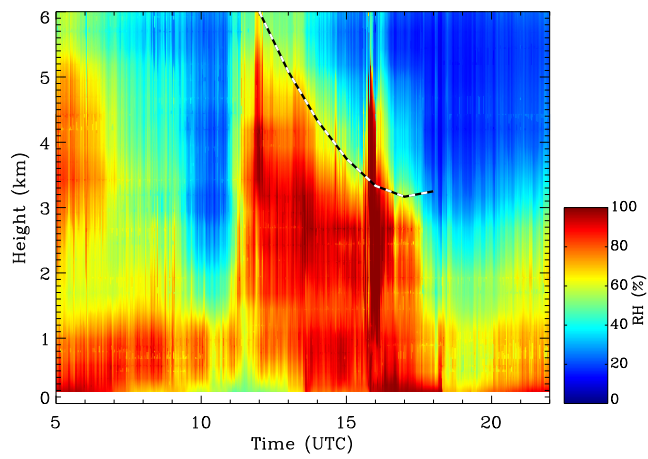
Figure 8. Vertical RH (%) profile from a UK Met Office Radio-metrics TP/WVP-3000 microwave radiometer that was located at Linkenholt. The dashed black and white line indicates the height of the base of the lowermost dry layer as identified by the Swanage radiosondes (Fig. 5).
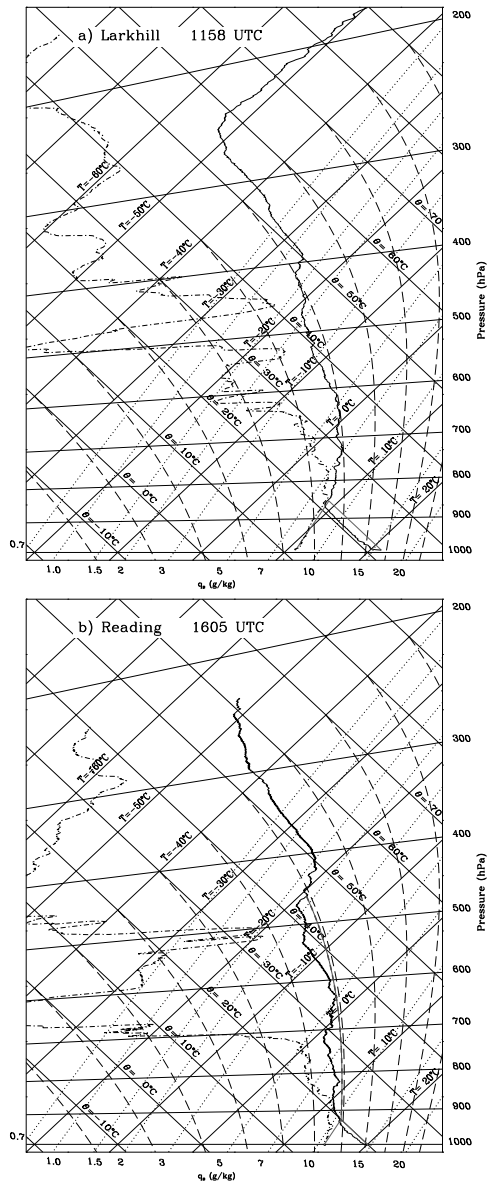
Figure 9. Dry bulb temperature (T; solid line) and dew-point temperature (T$_d$; dot-dashed line) measured by radiosondes launched from : a) Larkhill at 1158 UTC; and b) Reading at 1605 UTC. The lifting condensation level (LCL) has been plotted onto these soundings (i.e. where the solid grey lines starting from the surface T and T$_d$ meet when, respectively, the dry adiabat and the line of constant mixing ratio are followed upwards) and, in the case of Fig. 9(b), the vertical parcel trajectory (dashed grey line) has been continued from the LCL up the moist adiabat to show that the surface parcel would have reached about 450 hPa. It should also be noted that as a result of the irregular radiosonde launch times during this IOP, we are not able to illustrate the two phases of this case using soundings from the same location. However, Larkhill and Reading are relatively close (see Fig. 1) and would be influenced by the same surface and upper-level conditions due to the eastward flow of the major features being investigated here.
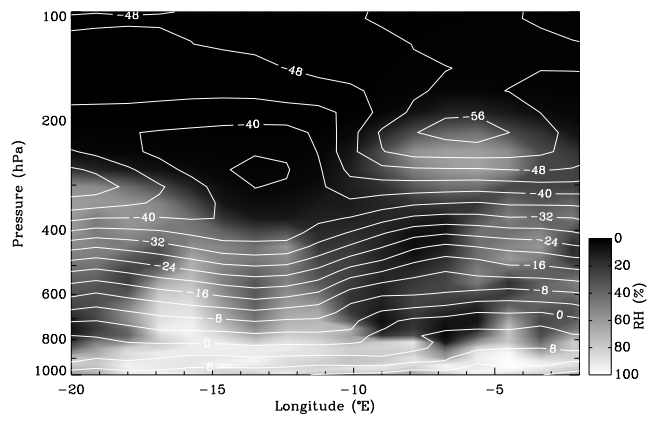
Figure 10. Relative humidity (RH; shading) and temperature (°C; white contours with an interval of 4°C) from the ECMWF operational analyses at 1200 UTC on 18 July 2005. This plot is a cross section through the dashed line seen in Fig. 2(c) i.e. from 20°W, 64°N to 2°W, 46°N.
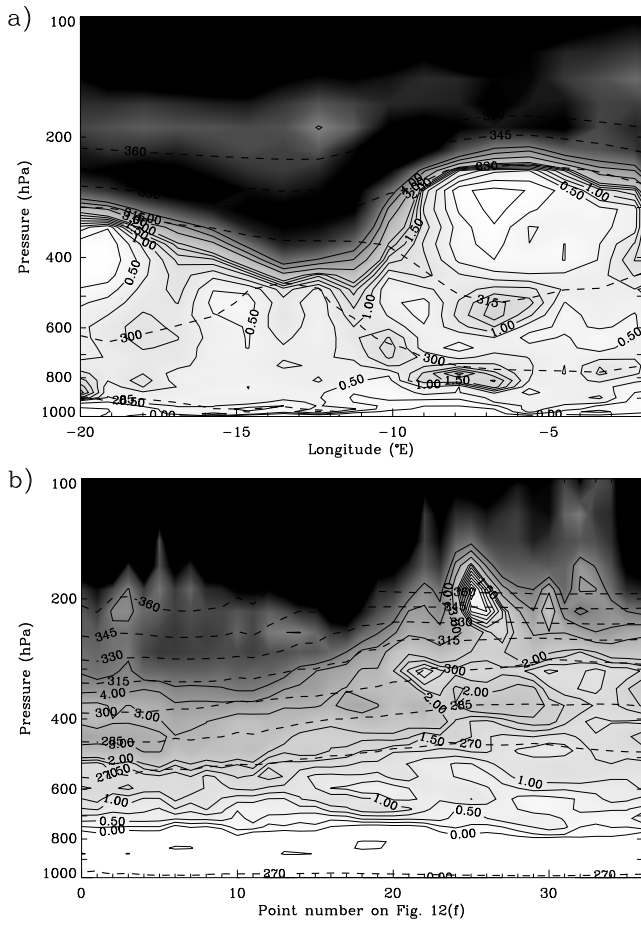
a)

b)

Figure 11. PV (in PVU; solid contours and shading; contour interval is 0.25 PVU below 2 PVU, and 1 PVU above 2 PVU; and darker shading relates to higher PV) and potential temperature (θ; dashed contours; contour interval is 15 K) from the ECMWF operational analyses at 1200 UTC for Figs. 11(a) and 0600 UTC for Fig. 11(b) on 18 July 2005. These data are plotted as cross sections through: a) the dashed line seen in Fig. 2(c) i.e. from 20°W, 64°N to 2°W, 46°N; and b) along the curved path shown by the circular points plotted on Fig. 12(f).
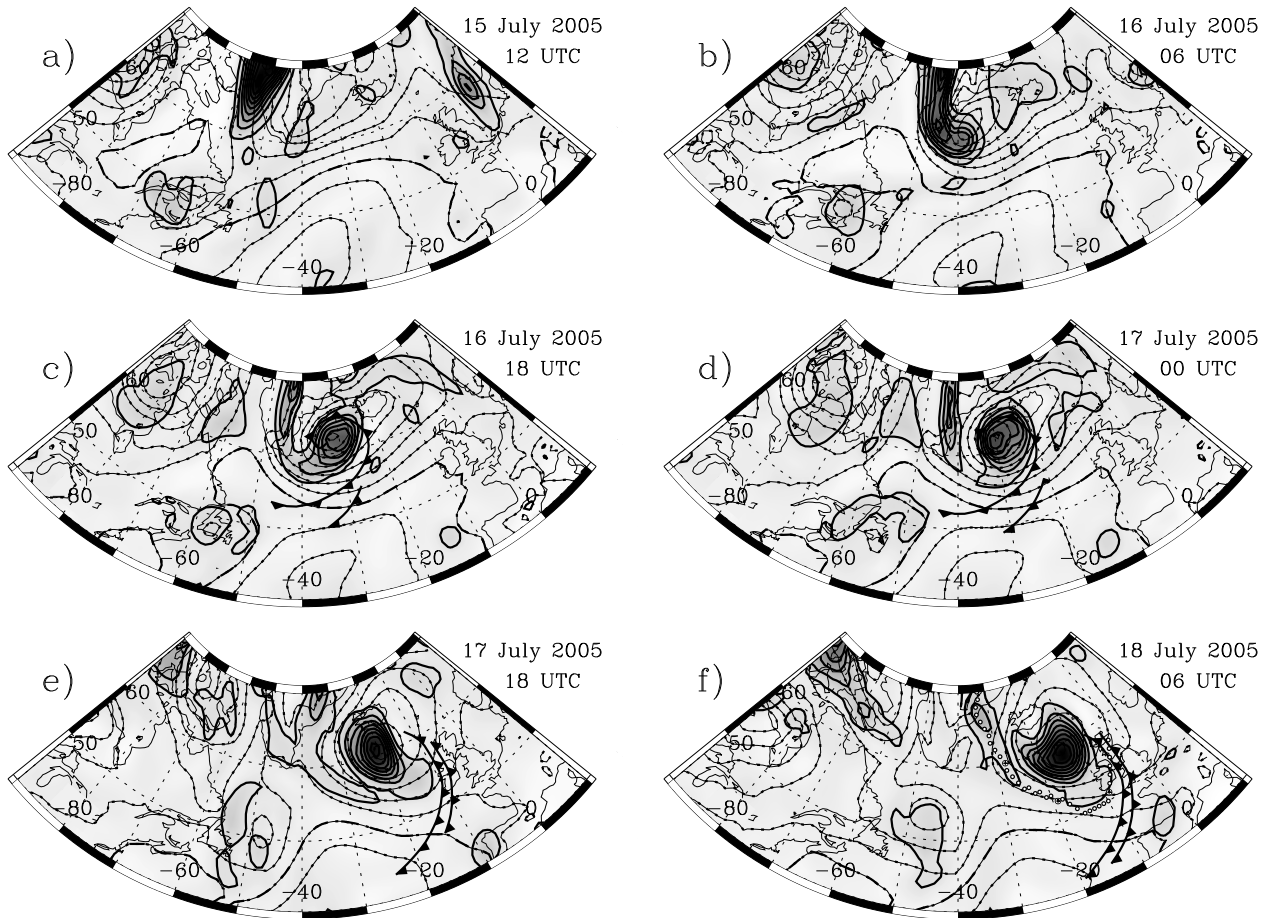
Figure 12. A selection of ECMWF operational analyses of PV (thick contours and shading) on the 315 K isentropic surface for the build up to the descending layers of upper-level air moving over the UK on the 18 July 2005. The contour interval is 1 PVU (i.e. 1.0×10^{-6} m^2 s^{-1} K kg^{-1}) and darker regions of shading show areas of higher PV. ECMWF operational analyses mean sea-level pressure (MSLP) is also plotted here (dotted contours; contour interval is 5 hPa; dash-dotted contour, for reference, is the 1020 hPa isobar). The position of relevant fronts (there were other fronts present for each time shown) from the Met Office surface analyses are plotted as well. The dots plotted on Fig. 12(f) relate to the grid points used to plot the vertical PV cross-section shown in Fig. 11(d). Point number (as used on the x-xaxis of Fig. 11(d)) increases from 0 in the north-west to 36 in the south-east. Points 10, 20 and 30 can be identified by being bigger than the other points and they have a cross plotted on them.
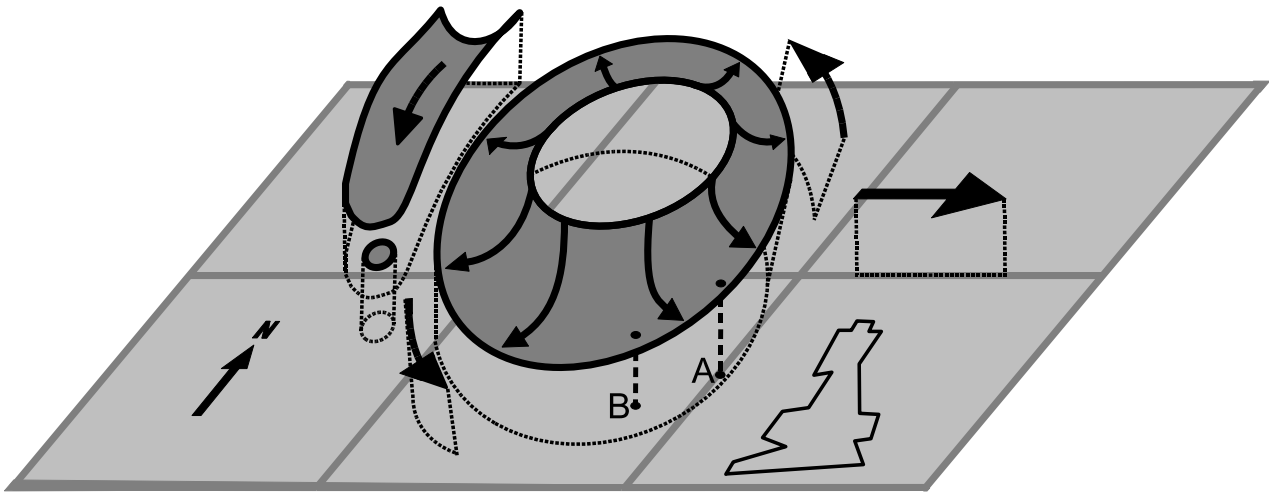
Figure 13. Schematic of a PV isosurface (approximately 1 PVU) based on the evidence presented in this paper. The schematic represents the tropospheric PV structure at approximately 0000 UTC on 18 July 2005 — a sketch of mainland Britain has been included to indicate the scale and location the the PV isosurface. Elevated features are shaded dark grey and the ground is shaded light grey. The sloping round/annular shaped feature in the centre of the drawing shows the downward flow in the upper-troposphere from the base of the main PV anomaly. The base of the round feature was higher in the north than in the south; this is indicated by the dotted lines (vertical and horizontal) that show how the features would translate onto the ground. The arrows indicate that the round feature was moving eastwards and rotating anti-clockwise but, because of the north to south slope, it was precessing around a moving axis rather than around a fixed vertical axis. Under these circumstances, observations taken from a fixed point beneath the round feature would show that it's base reduced in height over time. The points A and B plotted on Fig. 13 represent two such observations taken in the frame of reference stationary with respect to the rotating feature; this shows how an observer would see the base coming down in height, as was seen in this case. The streamer to the west of the main PV "skirt" has been plotted to show the source of the upper-most PV fragment that was observed during the case.